An Explicit Dynamic Model for Direct Reforming Carbonate Fuel Cell Stack

Michael D. Lukas, *Student Member, IEEE*, Kwang Y. Lee, *Senior Member, IEEE*, and Hossein Ghezel-Ayagh

***Abstract*—A nonlinear, lumped-parameter mathematical model of direct reforming carbonate fuel cell stack is extended by deriving an explicit set of differential equations for computer simulation. The equilibrium assumption used for the water–gas shift reaction results in an implicit equation set, previously solved using numerical techniques. An explicit equation set is derived by eliminating a key variable associated with the water–gas shift reaction. In addition, results are improved by incorporating a fuel cell performance model to account for reversible cell potential and polarization losses. This requires determination of intermediate gas composition at the cell anode inlet, resulting in additional computations. All results and physical data used are specific to a lumped 16-stack 2-MW system design, a precursor to a demonstration plant that had been operated at the City of Santa Clara, CA. Steady state results are validated for several load points over the upper region of operation and transient results are provided for sudden load change.**

***Index Terms*—Dynamics, fuel cells, power generation, simulation.**

I. Introduction

THE DIRECT Carbonate Fuel Cell (DFC) is a variant of molten carbonate fuel cells in that it internally reforms methane-containing fuels within the anode compartment of the fuel cell. DFC power plant is emerging as a viable highly efficient technology with net fuel-to-electricity efficiency of 55–60%. By utilizing waste heat in the higher temperature carbonate fuel cell, total thermal efficiencies can approach 85%. Emissions of CO_2 per pound of fuel are reduced due to the higher efficiencies while emissions of CO, NOx, and SOx are in the order of parts-per-million (PPM). Other benefits of fuel cell systems in general are the increased flexibility of sizing, fuel, and siting. Thus, with deregulation in electricity supply, new and existing energy suppliers have been attracted by the potential of fuel cell systems as distributed on-site generators.

The largest demonstration of molten carbonate fuel cell (MCFC) technology has been California's 2-MW Santa Clara Demonstration Project (SCDP) [1], [2]. The fuel cell stacks used in the SCDP were rated at 125-kW and based on "direct fuel-cell technology" developed by FuelCell Energy (FCE). Natural gas is internally reformed, partially in an internal reforming unit and partially at the cells, eliminating the need for a large external reforming unit to produce hydrogen fuel. The approach, Fig. 1, is a combination of indirect internal reforming (IIR) and direct internal reforming (DIR) which provides for better thermal management [3]. In FCEs design the internal reforming is achieved in two distinct steps. In the IIR step, a reforming unit (RU) containing nickel based catalyst is placed between every 10 fuel cells in the stack. The reforming units convert approximately 50–60 percent of the natural gas fuel to hydrogen prior to entry into the fuel cell anode. The partially reformed natural gas undergoes further reforming in the fuel cell anodes which are also loaded with reforming catalysts. This design approach ensures the benefits from the internal reforming concept are realized, including complete conversion of the natural gas to hydrogen, reduced fuel cell heat dissipation, and simplicity in design.

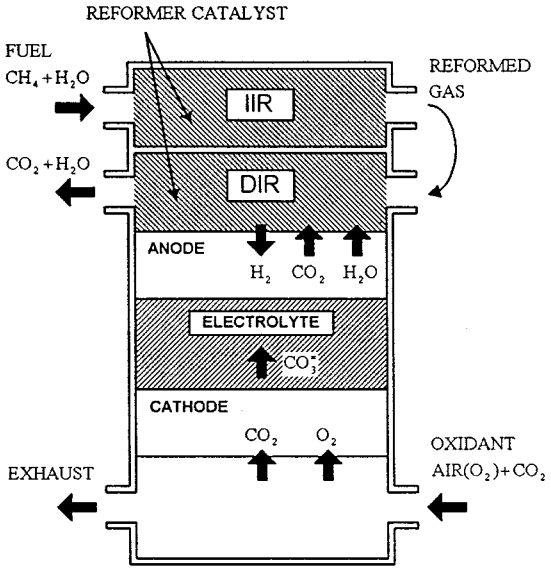

Fig. 1. IIR/DIR structure of MCFC stack.

A dynamic model for direct reforming carbonate fuel cell stack was derived in [4] to describe both short-term and long-term transient effects. Continuous stirred tank reactors (CSTRs) were used to describe both anode and cathode with the former lumping the combined effects of RU and cell anode. Fuel cell polarization losses were lumped into a single ohmic cell resistance. In this paper, the model is extended to include electrode polarization losses described by experimentally derived correlations dependent on gas composition at the cell anode inlet. This requires calculation of intermediate gas composition out of the RU, leaving the basic model unaffected.

Manuscript received February 14, 2000. This work is supported by the NSF grant "Intelligent Control and Dynamic Simulation of Molten Carbonate Fuel Cell Power Plants as Distributed Generation Systems" (DMI-9460694).

M. D. Lukas and K. Y. Lee are with the Department of Electrical Engineering, The Pennsylvania State University, University Park, PA 16802.

H. Ghezel-Ayagh is with FuelCell Energy, Inc., Danbury, CT 06813.

Publisher Item Identifier S 0885-8969(01)07337-5.

In the description of the model, anode inlet is used to denote the state of fuel at the RU inlet except when considering intermediate composition.

II. MCFC Stack Dynamic Model

Assuming a fuel cell stack temperature common to anode and cathode, ideal gases and mixtures, and energy storage only within the stack hardware, a single energy balance is written [4]:

$$M^s C_p^s \frac{dT^s}{dt} = N_{ta}^{\text{in}} \left[\sum_{i=1}^{\xi} x_{ai}^{\text{in}} \left(\overline{h}_{ai}^{\text{in}} - \overline{h}_i^s \right) \right] - \sum_{i=1}^{\xi} \overline{h}_i^s R_{ai} + N_{tc}^{\text{in}} \left[\sum_{i=1}^{\xi} x_{ci}^{\text{in}} \left(\overline{h}_{ci}^{\text{in}} - \overline{h}_i^s \right) \right] - \sum_{i=1}^{\xi} \overline{h}_i^s R_{ci} - P_{\text{dc}} \quad (1)$$

where

$M^s C_p^s$	stack solid mass-specific heat product [J/K];
T^s	stack solid average temperature [K];
$N_{ta}^{\text{in}}(N_{tc}^{\text{in}})$	anode (cathode) total inlet molar flow [mol/s];
$x_{ai}^{\text{in}}(x_{ci}^{\text{in}})$	anode (cathode) inlet mole fractions;
$\overline{h}_{ai}^{\text{in}}(\overline{h}_{ci}^{\text{in}})$	anode (cathode) inlet partial molar enthalpies [J/mol];
$\overline{h}_i^s$	partial molar enthalpies at stack temperature [J/mol];
ξ	total gas components in anode or cathode;
P_{dc}	stack dc power [W];
$R_{ai}(R_{ci})$	anode (cathode) total rate of production of species i [mol/s].

Under the ideal gas assumption the partial molar enthalpies are computed using

$$\overline{h}_i = \overline{h}_i^{ref} + \int_{T_{ref}}^{T} c_{p,i}(u)\, du$$

where coefficients of the specific heats $c_{p,i}$ [J/(kg · K)],

$$c_{p,i} = a_i + b_i T + c_i T^2 + d_i T^3$$

are found in standard reference tables. The reference enthalpy represents energy at standard reference temperature and includes the heat of formation for each gas species to account for energy change on chemical reaction. Total rates of production R_i can be written as

$$R_i = \sum_{j=1}^{\mu} \nu_{ij} r_j \quad (2)$$

where

μ	total number of chemical reactions;
r_j	rate of reaction j;
ν_{ij}	stoichiometric coefficient of gas species i in reaction j.

Gas component balances are:

Anode

$$\frac{dx_{ai}^s}{dt} = \frac{RT^s}{P_a^s V_a} \left[N_{ta}^{\text{in}}(x_{ai}^{\text{in}} - x_{ai}^s) - x_{ai}^s \sum_{i=1}^{\xi} R_{ai} + R_{ai} \right]. \quad (3a)$$

Cathode

$$\frac{dx_{ci}^s}{dt} = \frac{RT^s}{P_c^s V_c} \left[N_{ca}^{\text{in}}(x_{ci}^{\text{in}} - x_{ci}^s) - x_{ci}^s \sum_{i=1}^{\xi} R_{ci} + R_{ci} \right] \quad (3b)$$

where

$x_{ai}^s(x_{ci}^s)$	anode (cathode) outlet mole fractions;
$P_a^s(P_c^s)$	anode (cathode) outlet pressures [kg/(m · s^2)];
$V_a(V_c)$	anode (cathode) compartment volumes [m^3];
R	universal gas constant[J/(mol · K)].

Equations (1)–(3) are subject to the following reactions on the anode side:

$$\text{H}_2 + \text{CO}_3^{=} \longrightarrow \text{H}_2\text{O} + \text{CO}_2 + 2\text{e}^- \quad \textit{Anode} \quad (4)$$

$$\text{CO} + \text{H}_2\text{O} \longrightarrow \text{CO}_2 + \text{H}_2 \quad \textit{Water–Gas Shift} \quad (5)$$

$$\text{CH}_4 + \text{H}_2\text{O} \longrightarrow \text{CO} + 3\text{H}_2 \quad \textit{Reforming} \quad (6)$$

and on the cathode side:

$$\tfrac{1}{2}\,\text{O}_2 + \text{CO}_2 + 2\text{e}^- \longrightarrow \text{CO}_3^{=} \quad \textit{Cathode.} \quad (7)$$

The rates of electrochemical reactions (4) and (7) are equal and proportional to load current through Faraday's Law while the reforming reaction rate is dependent on temperature, pressure, and gas composition at the anode compartment [4]. However, the water–gas shift (WGS) reaction is assumed at equilibrium and therefore a reaction rate is undefined. Instead, the equilibrium assumption imposes a constraint on gas species at the anode compartment:

$$K_{seq} = e^{(E_1 + E_2/T^s)} = \frac{x_{\text{CO}_2}^s x_{\text{H}_2}^s}{x_{\text{CO}}^s x_{\text{H}_2\text{O}}^s} \quad (8)$$

where K_{seq} is the WGS equilibrium constant and E_1 and E_2 are related to Gibb's free energy change on the WGS reaction. With an undefined reaction rate, (2) and subsequently, (1) and (3) cannot be evaluated. In the following, this reaction rate is removed from the equation set.

III. Explicit Model Derivation

At the anode side there are three simultaneous reactions (4)–(6). In the following, these will be denoted as reactions 1, 2, and 3, respectively. The term corresponding to the total rate of production at the anode is rewritten:

$$R_{ai} = \sum_{j=1}^{3} \nu_{ij} r_j = \sum_{\substack{j=1 \\ j \neq 2}}^{3} \nu_{ij} r_j + \nu_{i2} r_2 \equiv \overline{R}_{ai} + \nu_{i2} r_2. \quad (9)$$

This considers r_2 as a legitimate variable and separates it for eventual elimination. The set of all gas species (anode or cathode) is first identified:

$$\mathbf{S} \equiv \{ \text{H}_2 \quad \text{CH}_4 \quad \text{CO} \quad \text{CO}_2 \quad \text{H}_2 \quad \text{O} \quad \text{N}_2 \quad \text{O}_2 \} \quad (10)$$

where the ordering is used to refer to individual gas species (e.g., x_4 is the mole fraction of CO_2). To simplify the development, the following definitions are made:

Anode Side Quantities

$$\overline{\mathbf{h}}_{\mathbf{a}}^{\mathbf{in}} \equiv \begin{bmatrix} \overline{h}_{a1}^{\text{in}} \\ \vdots \\ \overline{h}_{a7}^{\text{in}} \end{bmatrix}, \quad \mathbf{X}_{\mathbf{a}}^{\mathbf{in}} \equiv \begin{bmatrix} x_{a1}^{\text{in}} \\ \vdots \\ x_{a7}^{\text{in}} \end{bmatrix},$$

$$\overline{\mathbf{R}}_\mathbf{a} \equiv \begin{bmatrix} \overline{R}_{a1} \\ \vdots \\ \overline{R}_{a7} \end{bmatrix}, \quad \boldsymbol{\nu_2} \equiv \begin{bmatrix} \nu_{12} \\ \vdots \\ \nu_{72} \end{bmatrix}.$$

Cathode Side Quantities

$$\overline{\mathbf{h}}_\mathbf{c}^{\,\mathbf{in}} \equiv \begin{bmatrix} \overline{h}_{c1}^{\,\mathrm{in}} \\ \vdots \\ \overline{h}_{c7}^{\,\mathrm{in}} \end{bmatrix}, \quad \mathbf{X}_\mathbf{c}^{\,\mathbf{in}} \equiv \begin{bmatrix} x_{c1}^{\,\mathrm{in}} \\ \vdots \\ x_{c7}^{\,\mathrm{in}} \end{bmatrix}, \quad \mathbf{R}_\mathbf{c} \equiv \begin{bmatrix} R_{c1} \\ \\ \vdots \\ \\ R_{c7} \end{bmatrix}. \quad (11)$$

Additional Quantities

$$\overline{\mathbf{h}}^{\,\mathbf{s}} \equiv \begin{bmatrix} \overline{h}_1^{\,s} \\ \vdots \\ \overline{h}_7^{\,s} \end{bmatrix}, \quad \boldsymbol{\Delta\overline{h}}_\mathbf{a} \equiv \overline{\mathbf{h}}_\mathbf{a}^{\,\mathbf{in}} - \overline{\mathbf{h}}^{\,\mathbf{s}}, \quad \boldsymbol{\Delta\overline{h}}_\mathbf{c} \equiv \overline{\mathbf{h}}_\mathbf{c}^{\,\mathbf{in}} - \overline{\mathbf{h}}^{\,\mathbf{s}}.$$

On the anode side, the component balance (3a) for CO is arbitrarily chosen to express r_2 by substituting (9) into (3a) and rewriting. The mole fraction for CO is explicitly denoted and the a subscript is dropped:

$$r_2 = \frac{\left\{ \dfrac{V_a P_a^s}{RT^s} \dfrac{dx_{\mathrm{CO}}^s}{dt} - \mathrm{N}_{ta}^{\mathrm{in}} \left(x_{\mathrm{CO}}^{\mathrm{in}} - x_{\mathrm{CO}}^s \right) + x_{\mathrm{CO}}^s \sum_{i=1}^{\xi} \overline{R}_{ai} - \overline{R}_{a3} \right\}}{(\nu_{32} - x_{\mathrm{CO}}^s \overline{\nu}_2)}. \quad (12)$$

In (12) the following definition has been used:

$$\overline{\nu}_2 \equiv \sum_{i=1}^{\xi} \nu_{i2}. \quad (13)$$

Equation (12) is then re-substituted into (3a), eliminating r_2, where all remaining component balances ($i \neq 3$) on the anode side are in terms of x_{CO}^s and $\dot{x}_{\mathrm{CO}}^s$:

$$\begin{aligned} &\frac{V_a P_a^s}{RT^s} \frac{dx_{ai}^s}{dt} \\ &\quad = N_{ta}^{\mathrm{in}} (x_{ai}^{\mathrm{in}} - x_{ai}^s) - x_{ai}^s \sum_{i=1}^{\xi} \overline{R}_{ai} + \overline{R}_{ai} + \frac{(\nu_{i2} - x_{ai}^s \overline{\nu}_2)}{(\nu_{32} - x_{\mathrm{CO}}^s \overline{\nu}_2)} \\ &\qquad \times \left[\frac{V_a P_a^s}{RT^s} \frac{dx_{\mathrm{CO}}^s}{dt} - N_{ta}^{\mathrm{in}} (x_{\mathrm{CO}}^{\mathrm{in}} - x_{\mathrm{CO}}^s) + x_{\mathrm{CO}}^s \sum_{i=1}^{\xi} \overline{R}_{ai} - \overline{R}_{a3} \right]. \end{aligned} \quad (14)$$

From the definition in (11) and inspection of the WGS reaction,

$$\boldsymbol{\nu_2} = [1 \quad 0 \quad -1 \quad 1 \quad -1 \quad 0 \quad 0]',$$

where positive and negative coefficients represent products and reactants, respectively. From (13), then $\overline{\nu}_2 = 0$. This implies that the bracketed term in (14) is multiplied by zero when $i = 2$, 6, or 7. In other words, the mole balance equations for CH_4, N_2, and O_2 do not involve x_{CO}^s or $\dot{x}_{\mathrm{CO}}^s$. Thus, a coupled set of differential equations exists among $x_{\mathrm{H_2}}^s$, x_{CO}^s, $x_{\mathrm{CO_2}}^s$, $x_{\mathrm{H_2O}}^s$, and T^s. To see the coupling with stack temperature, (12) is substituted into the energy balance (1) where the relationships in (11) have been used:

$$\begin{aligned} &M^s C_p^s \frac{dT^s}{dt} \\ &\quad = N_{ta}^{\mathrm{in}} \left(\boldsymbol{\Delta\overline{h}}_\mathbf{a}^{\,\mathbf{in}} \cdot \mathbf{X}_\mathbf{a}^{\,\mathbf{in}} \right) + N_{ca}^{\mathrm{in}} \left(\boldsymbol{\Delta\overline{h}}_\mathbf{c}^{\,\mathbf{in}} \cdot \mathbf{X}_\mathbf{c}^{\,\mathbf{in}} \right) \\ &\qquad - \left(\overline{\mathbf{h}}^{\,\mathbf{s}} \cdot \overline{\mathbf{R}}_\mathbf{a} \right) - \left(\overline{\mathbf{h}}^{\,\mathbf{s}} \cdot \mathbf{R}_\mathbf{c} \right) - P_{\mathrm{dc}} - \frac{\left(\overline{\mathbf{h}}^{\,\mathbf{s}} \cdot \boldsymbol{\nu_2} \right)}{(\nu_{32} - x_{\mathrm{CO}}^s \overline{\nu}_2)} \\ &\qquad \times \left[\frac{V_a P_a^s}{RT^s} \frac{dx_{\mathrm{CO}}^s}{dt} - N_{ta}^{\mathrm{in}} (x_{\mathrm{CO}}^{\mathrm{in}} - x_{\mathrm{CO}}^s) \right. \\ &\qquad\quad \left. + x_{\mathrm{CO}}^s \sum_{i=1}^{\xi} \overline{R}_{ai} - \overline{R}_{a3} \right]. \end{aligned} \quad (15)$$

Equations (14) and (15) form an implicit equation set. To transform these into an explicit set, the WGS equilibrium constraint (8) is first differentiated with respect to time. Since all quantities are still on the anode side, the subscript a is again dropped:

$$\begin{aligned} \frac{dx_{\mathrm{CO}}^s}{dt} = &\frac{x_{\mathrm{CO}}^s}{x_{\mathrm{H_2}}^s} \frac{dx_{\mathrm{H_2}}^s}{dt} + \frac{x_{\mathrm{CO}}^s}{x_{\mathrm{CO_2}}^s} \frac{dx_{\mathrm{CO_2}}^s}{dt} \\ &- \frac{x_{\mathrm{CO}}^s}{x_{\mathrm{H_2O}}^s} \frac{dx_{\mathrm{H_2O}}^s}{dt} + \frac{x_{\mathrm{CO}}^s E_2}{(T^s)^2} \frac{dT^s}{dt}. \end{aligned} \quad (16)$$

Finally, substituting $\dot{x}_{\mathrm{H_2O}}^s$, $\dot{x}_{\mathrm{CO_2}}^s$, and $\dot{x}_{\mathrm{H_2}}^s$ from (14), and $\dot{T}^s$ from (15), each into (16), an equation involving only one derivative ($\dot{x}_{\mathrm{CO}}^s$) can be isolated and written explicitly. This can then be back-substituted into (14) and (15) to complete an explicit set. A similar derivation is not necessary for cathode side quantities since there is only the electrochemical reaction (7). Before presenting the final results, some terms are evaluated by inspection of (4)–(7):

$$\begin{aligned} \overline{\mathbf{R}}_\mathbf{a} &= [-r_1 + 3r_3 \quad -r_3 \quad r_3 \quad r_1 \quad r_1 - r_3 \quad 0 \quad 0]', \\ \mathbf{R}_\mathbf{c} &= [0 \quad 0 \quad 0 \quad -r_1 \quad 0 \quad 0 \quad -\tfrac{1}{2} r_1]', \\ \sum_{i=1}^{7} \overline{R}_{ai} &= r_1 + 2r_3, \quad \text{and} \quad \sum_{i=1}^{7} R_{ci} = -\tfrac{3}{2} r_1. \end{aligned}$$

A number of additional quantities are defined:

$$\begin{aligned} \alpha_1 &\equiv x_{\mathrm{CO}}^s \left[\frac{1}{x_{\mathrm{CO}}^s} + \frac{1}{x_{\mathrm{CO_2}}^s} + \frac{1}{x_{\mathrm{H_2}}^s} + \frac{1}{x_{\mathrm{H_2O}}^s} \right] \\ \alpha_2 &\equiv \frac{-V_a P_a^s x_{\mathrm{CO}}^s E_2 (\overline{\mathbf{h}}^{\,\mathbf{s}} \cdot \boldsymbol{\nu_2})}{(T^s)^3 R M^s C_p^s} \\ \alpha_3 &\equiv N_{ta}^{\mathrm{in}} + r_1 + 2r_3 \\ \alpha_4 &\equiv \frac{RT^s}{V_a P_a^s} \\ \alpha_5 &\equiv \frac{RT^s}{V_c P_c^s} \\ \lambda_1 &\equiv \frac{1}{\alpha_1 + \alpha_2} \\ \lambda_2 &\equiv \frac{E_2 x_{\mathrm{CO}}^s}{(T^s)^2 M_s C_p^s} \left\{ N_{ta}^{\mathrm{in}} \left(\boldsymbol{\Delta\overline{h}}_\mathbf{a} \cdot \mathbf{X}_\mathbf{a}^{\,\mathbf{in}} \right) + N_{tc}^{\mathrm{in}} \left(\boldsymbol{\Delta\overline{h}}_\mathbf{c} \cdot \mathbf{X}_\mathbf{c}^{\,\mathbf{in}} \right) \right. \\ &\qquad \left. - \left(\overline{\mathbf{h}}^{\,\mathbf{s}} \cdot \overline{\mathbf{R}}_\mathbf{a} \right) - \left(\overline{\mathbf{h}}^{\,\mathbf{s}} \cdot \mathbf{R}_\mathbf{c} \right) + \left(\overline{\mathbf{h}}^{\,\mathbf{s}} \cdot \boldsymbol{\nu_2} \right) \right. \end{aligned}$$

$$\cdot\left[\alpha_3 x^s_{\mathrm{CO}} - N^{\mathrm{in}}_{ta} x^{\mathrm{in}}_{\mathrm{CO}} - r_3\right] - P_{\mathrm{dc}}\Big\}$$

$$-\alpha_4 x^s_{\mathrm{CO}}\left\{\begin{array}{l}\dfrac{1}{x^s_{\mathrm{CO_2}}}\left[\alpha_3(x^s_{\mathrm{CO_2}}+x^s_{\mathrm{CO}}) - N^{\mathrm{in}}_{ta}\right.\\ \qquad\left.\cdot\left(x^{\mathrm{in}}_{\mathrm{CO_2}}+x^{\mathrm{in}}_{\mathrm{CO}}\right) - r_1 - r_3\right]\\ +\dfrac{1}{x^s_{\mathrm{H_2}}}\left[\alpha_3\left(x^s_{\mathrm{H_2}}+x^s_{\mathrm{CO}}\right) - N^{\mathrm{in}}_{ta}\right.\\ \qquad\left.\cdot\left(x^{\mathrm{in}}_{\mathrm{H_2}}+x^{\mathrm{in}}_{\mathrm{CO}}\right) - 4r_3 + r_1\right]\\ -\dfrac{1}{x^s_{\mathrm{H_2O}}}\left[\alpha_3\left(x^s_{\mathrm{H_2O}}-x^s_{\mathrm{CO}}\right) - N^{\mathrm{in}}_{ta}\right.\\ \qquad\left.\cdot\left(x^{\mathrm{in}}_{\mathrm{H_2O}}-x^{\mathrm{in}}_{\mathrm{CO}}\right) - r_1 + 2r_3\right]\end{array}\right\}$$

$$\lambda_3 \equiv \frac{1}{M_s C^s_p}\left\{N^{\mathrm{in}}_{ta}\left(\boldsymbol{\Delta\overline{h}_a}\cdot\mathbf{X^{in}_a}\right) + N^{\mathrm{in}}_{tc}\left(\boldsymbol{\Delta\overline{h}_c}\cdot\mathbf{X^{in}_c}\right) - \left(\overline{\mathbf{h}}^{\mathbf{s}}\cdot\overline{\mathbf{R}}_{\mathbf{a}}\right) - \left(\overline{\mathbf{h}}^{\mathbf{s}}\cdot\mathbf{R_c}\right) + \left(\overline{\mathbf{h}}^{\mathbf{s}}\cdot\boldsymbol{\nu_2}\right) \cdot\left[\frac{\lambda_1\lambda_2}{\alpha_4} + \alpha_3 x^s_{\mathrm{CO}} - N^{\mathrm{in}}_{ta}x^{\mathrm{in}}_{\mathrm{CO}} - r_3\right] - P_{\mathrm{dc}}\right\}.$$

Using the above definitions an explicit set of equations describing fuel cell dynamics follows:

Anode Composition

$$\frac{dx^s_{\mathrm{H_2}}}{dt} = -\alpha_4\left\{\alpha_3\left(x^s_{\mathrm{H_2}}+x^s_{\mathrm{CO}}\right) - N^{\mathrm{in}}_{ta} \cdot\left(x^{\mathrm{in}}_{\mathrm{H_2}}+x^{\mathrm{in}}_{\mathrm{CO}}\right) - 4r_3 + r_1\right\} - \lambda_1\lambda_2$$

$$\frac{dx^s_{\mathrm{CH_4}}}{dt} = -\alpha_4\left\{\alpha_3 x^s_{\mathrm{CH_4}} - N^{\mathrm{in}}_{ta}x^{\mathrm{in}}_{\mathrm{CH_4}} + r_3\right\}$$

$$\frac{dx^s_{\mathrm{CO}}}{dt} = \lambda_1\lambda_2$$

$$\frac{dx^s_{\mathrm{CO_2}}}{dt} = -\alpha_4\left\{\alpha_3\left(x^s_{\mathrm{CO_2}}+x^s_{\mathrm{CO}}\right) - N^{\mathrm{in}}_{ta} \cdot\left(x^{\mathrm{in}}_{\mathrm{CO_2}}+x^{\mathrm{in}}_{\mathrm{CO}}\right) - r_1 - r_3\right\} - \lambda_1\lambda_2$$

$$x^s_{\mathrm{H_2O}} = \frac{x^s_{\mathrm{CO_2}}x^s_{\mathrm{H_2}}}{K_{seq}x^s_{\mathrm{CO}}}$$

$$x^s_{N_2} = 1 - \left(x^s_{\mathrm{H_2}} + x^s_{\mathrm{CH_4}} + x^s_{\mathrm{CO}} + x^s_{\mathrm{CO_2}} + x^s_{\mathrm{H_2O}}\right).$$

Stack Temperature

$$\frac{dT^s}{dt} = \lambda_3.$$

Cathode Composition

$$\frac{dx^s_{\mathrm{H_2O}}}{dt} = \alpha_5\left\{N^{\mathrm{in}}_{tc}\left(x^{\mathrm{in}}_{\mathrm{H_2O}} - x^s_{\mathrm{H_2O}}\right) + \frac{3x^s_{\mathrm{H_2O}}r_1}{2}\right\}$$

$$\frac{dx^s_{\mathrm{CO_2}}}{dt} = \alpha_5\left\{N^{\mathrm{in}}_{tc}\left(x^{\mathrm{in}}_{\mathrm{CO_2}} - x^s_{\mathrm{CO_2}}\right) + \frac{3x^s_{\mathrm{CO_2}}r_1}{2} - r_1\right\}$$

$$\frac{dx^s_{N_2}}{dt} = \alpha_5\left\{N^{\mathrm{in}}_{tc}\left(x^{\mathrm{in}}_{N_2} - x^s_{N_2}\right) + \frac{3x^s_{N_2}r_1}{2}\right\}$$

$$x^s_{O_2} = 1 - \left(x^s_{\mathrm{CO_2}} + x^s_{\mathrm{H_2O}} + x^s_{N_2}\right).$$

Included in these equations are the facts that mole fractions sum to unity and that certain gas species are not present. Expressions for the reaction rates r_1 and r_3 are given in [4]. To complete the model, two additional state equations are used to describe anode and cathode pressures. These are derived by differentiating the ideal gas law $\tilde{C}_t = P^s/RT^s$ with respect to time, where $\tilde{C}_t$ is total concentration [mol/m^3], and using a total mole balance [4] to eliminate $d\tilde{C}_t/dt$ for both anode and cathode. This results in:

$$\frac{dP^s_a}{dt} = \frac{RT^s}{V_a}\left[N^{\mathrm{in}}_{ta} - N^o_{ta} + r_1 + 2r_3 + \frac{\lambda_3 V_a P^s_a}{(T^s)^2 R}\right] \qquad \textit{Anode}$$

$$\frac{dP^s_c}{dt} = \frac{RT^s}{V_c}\left[N^{\mathrm{in}}_{tc} - N^o_{tc} - \frac{3r_1}{2} + \frac{\lambda_3 V_c P^s_c}{(T^s)^2 R}\right] \qquad \textit{Cathode}$$

where N^o_{ta} and N^o_{tc} are the anode and cathode exhaust total molar flows, respectively.

IV. Cell Voltage Representation

Cell voltage under load current i [A/cm^2] is expressed as [5]:

$$V_{cell} = V_o - \eta_{act} - \eta_{conc} - iz \tag{17}$$

where

- V_o equilibrium potential [V];
- η_{act} activation polarization [V];
- η_{conc} concentration polarization [V];
- z cell ohmic impedance [$\Omega\cdot$cm^2].

Activation polarization is caused by electrode kinetics while concentration polarization is caused by concentration gradients in the electrode. Equilibrium potential is described by the Nernst equation [5]:

$$V_o = E_o + \frac{RT}{2F}\cdot\ln\frac{P_{\mathrm{H_2},a}P^{1/2}_{\mathrm{O_2},c}P_{\mathrm{CO_2},c}}{P_{\mathrm{H_2O},a}P_{\mathrm{CO_2},a}} \tag{18}$$

where

- E_o standard potential [V];
- F Faraday's constant [J/(mol $\cdot$ V)];
- P_i partial pressure ($P_{i,a} \equiv x_{ai}P_a/P_{atm}$, $P_{i,c} \equiv x_{ci}P_c/P_{atm}$).

Partial pressures (normalized to atmospheric pressure P_{atm}) depend on anode/cathode gas pressure and composition while standard potential and ohmic impedance are both temperature dependent. Fuel cell polarization losses are generally dependent on partial pressures, temperature, and current density, and are spatially distributed in an actual cell. In this study the dynamic model is lumped parameter, CSTR-type where outlet properties are equal to average properties. A fuel cell performance model, correlated with experimental data [6], is incorporated in the dynamic model in order to predict the DC voltage as a function of state variables.

Standard Potential

$$E_o = \frac{4184\times[58.3 - (0.0113 + 9.6\times10^{-7}T)T]}{2F}.$$

Activation Polarization

$$\eta_{act} = \frac{RT}{2F}(-21 - 0.31\ln P_{\mathrm{H_2},a} - 0.24\ln P_{\mathrm{CO_2},a} - 0.95\ln P_{\mathrm{H_2O},a} + 0.86\ln P_{\mathrm{CO_2},c} - 1.8\ln P_{\mathrm{O_2},c} + 7050/T - 2.6\ln i).$$

Concentration Polarization

$$\eta_{conc} = -1.22 \ln\left(1 - \frac{i}{0.64}\right).$$

Cell Ohmic Impedance

$$z = 0.4 \exp\left[-2870\left(\frac{1}{923} - \frac{1}{T}\right)\right].$$

In the equation above, T is the arithmetic average of cathode inlet and exit temperature [K] and i is current [A/cm^2]. Anode and cathode partial pressures are arithmetic averages of inlet and exit gas partial pressures, where anode inlet gas is assumed to be *pre-equilibrated* to account for gas composition change within the reforming unit. With these considerations in mind, a number of assumptions are made linking the performance model to the lumped-parameter model:

$$T = (T^s + T_c^{\text{in}})/2 \tag{A1}$$

$$P_{i,c} = P_c^s (x_{ci}^s + x_{ci}^{\text{in}})/2 \tag{A2}$$

$$P_{i,a} = P_a^s (x_{ai}^s + x_{ai}^{ru})/2 \tag{A3}$$

where x_{ai}^{ru} denotes anode inlet (RU exit) mole fraction. This is calculated by assuming the WGS and reforming reactions at equilibrium corresponding to the following pre-equilibrium temperature and pre-equilibrium pressure:

$$T_{ref} = T_a^{\text{in}} \tag{A4}$$

$$P_{ref} = P_a^s. \tag{A5}$$

In (A2), (A3), and (A5), cell inlet pressure is not used in the averaging, thus avoiding complicated hydrodynamic pressure/flow models. Calculation of x_{ai}^{ru} then becomes a standard equilibrium problem [7], solved at each integration time step by a Newton–Raphson iteration. Assumptions (A1)–(A5) are also used to calculate the second term in the Nernst equation (18).

V. Simulation Results

Parameters used in the dynamic model were obtained from FCEs 2-MW conceptual system design leading to the Santa Clara Demonstration Project (SCDP) and include: anode and cathode volumes, stack solid mass and specific heat, cell active area, and reforming catalyst surface area. All parameters correspond to a 16-stack equivalent. Standard constants were used corresponding to WGS and reforming reactions. System voltage in the SCDP is taken across a series connection of four stacks, each stack consisting of 258 cells ($V_{sys} = 4 \times 258 \times V_{cell}$). Table I shows a steady state comparison of model and plant data [8]. Here, the model voltage was computed open-loop (no inverter) subject to the actual plant load current.

To investigate transient behavior, the plant is assumed to be at steady state corresponding to rated power (1964 kW gross dc) and subjected to a sudden increase in power demand. The setup in Fig. 2 is assumed, where the balance-of-plant, power conditioning system (PCS), and plant control system are included in the simulation [9]. The inverter is assumed to regulate bus voltage perfectly (with unity power factor) and simply draws

TABLE I
Steady State Simulation Results

	Load current [A]	System Voltage [V]	
		Plant	Model
Full power	3056	750	720
Rated power	2483	791	777
Part load	2101	816	812

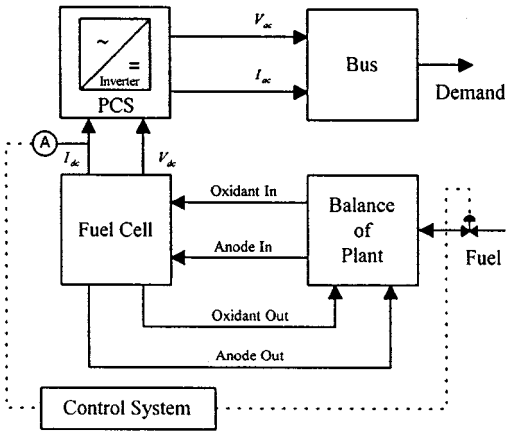

Fig. 2. SCDP plant simulation.

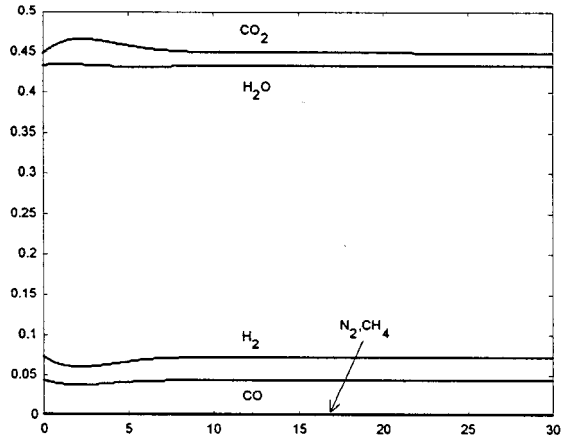

Fig. 3. Anode gas composition.

stack current proportional to bus current and inversely proportional to stack voltage using a power demand setpoint. Stack current is measured and used in calculation of fuel flow setpoint to maintain 75% fuel utilization (fraction of total fuel that reacts electrochemically). All controls loops are operational and include: stack differential pressure, stack temperature, steam-to-carbon ratio, etc. [9]. Figs. 3–8 show the responses to a 10% step-up in power demand.

Anode gas composition, Fig. 3, changes quickly (fast control of fuel flow) in response to the disturbance and returns to its original value corresponding to 75% fuel utilization, Fig. 4. Anode and cathode pressures in Fig. 5 both increase as a result of the increased load. Differential pressure between anode and cathode is controlled by the booster blower [9] with a setpoint of

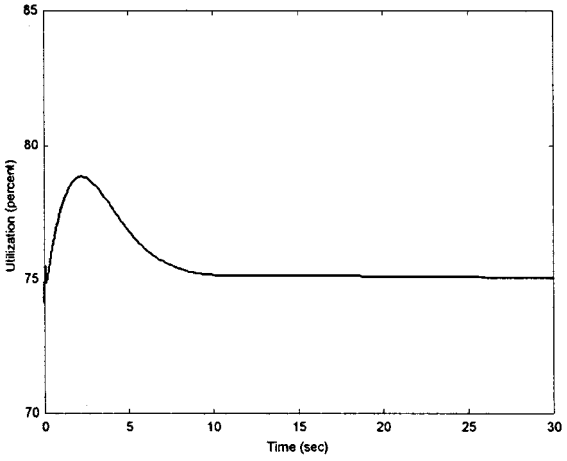

Fig. 4. Fuel utilization.

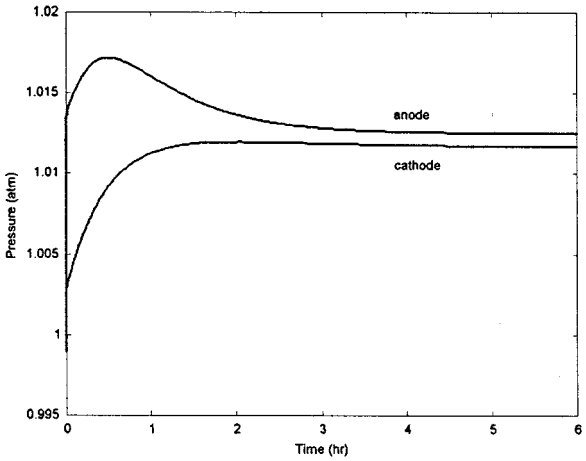

Fig. 5. Anode and cathode pressures.

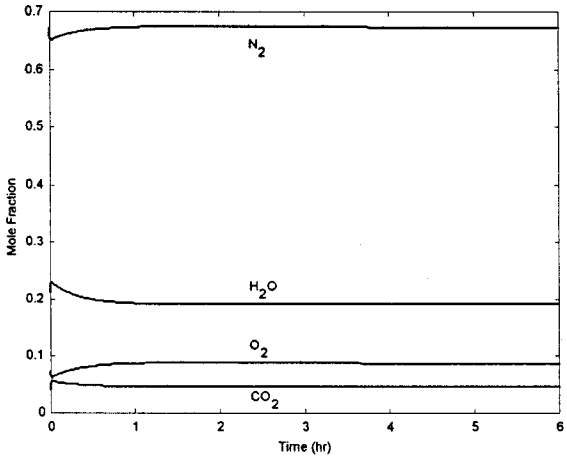

Fig. 6. Cathode gas composition.

0.012 psia. Unlike the anode, cathode gas composition, Fig. 6, is not nearly invariant under load changes. This is due to the stack temperature control system which increases the air flow rate to the cathode, consequently increasing oxygen and nitrogen mole fractions. The large response time in Figs. 5–8, is a result of

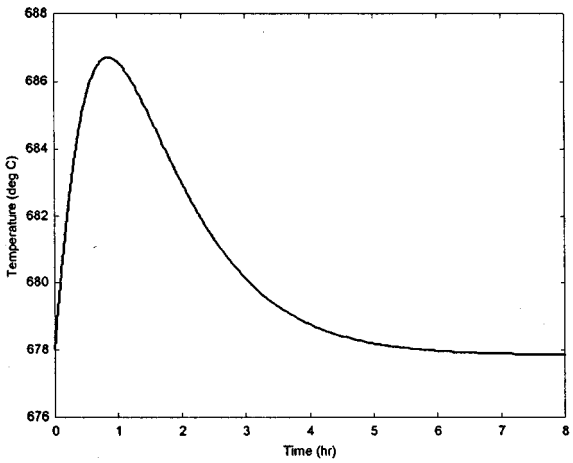

Fig. 7. Stack temperature.

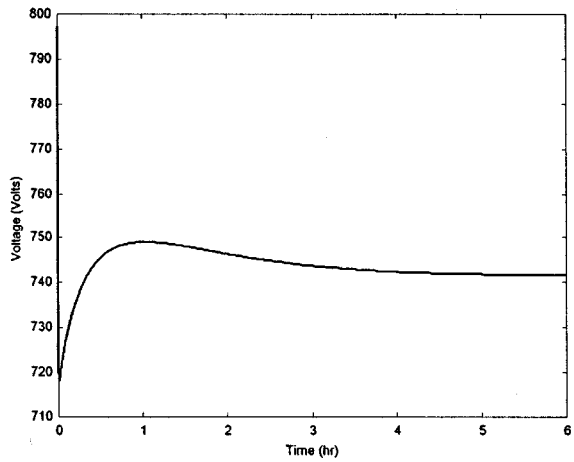

Fig. 8. System voltage.

the 16-stack mass-specific heat product in (1), the thermal time constant of stack temperature, Fig. 7. System voltage in Fig. 8 starts at its initial value of 797 V, corresponding to regulated power (inverter control), and drops quickly to a sudden increase in stack current, in turn, controlled by the inverter to maintain the new power setpoint. System (stack) voltage varies according to the temperature dependence in (18) while stack current is continuously adjusted by the inverter control to maintain power.

VI. Conclusion

A 10-state, explicit dynamic model for direct reforming DFC stack was derived for computer simulation. The reaction rate corresponding to the WGS reaction at equilibrium was undefined and eliminated from the equation set. The results were then manipulated to obtain an explicit set of differential equations. The dynamic model results were improved by including correlations from a validated three-dimensional performance model. Several load points were used for comparison between plant and model. A balance-of-plant/control system model was included in the simulation and transient results were analyzed for a step change in power demand. Design data and physical parameters have been based on a 2-MW demonstration power plant.

REFERENCES

[1] T. P. O'Shea and A. J. Leo, "The Santa Clara demonstration project 2-MW direct carbonate fuel cell power plant," in *29th IECEC Meeting*, Monterey, CA, 1994, pp. 817–822.

[2] M. Monn, "Project brings fuel cell closer to utility use," *Power*, vol. 139, no. 4, pp. 76–79, Apr. 1995.

[3] M. Farooque, "Development of internal reforming carbonate fuel cell technology, final report," prepared for U.S. DOE/METC, DOE/MC/23 274-2941, pp. 3–6 to 3–11, Oct. 1991.

[4] M. D. Lukas, K. Y. Lee, and H. Ghezel-Ayagh, "Development of a stack stimulation model for control study on direct reforming molten carbonate fuel cell power plant," *IEEE Trans. Energy Conversion*, vol. 14, no. 4, pp. 1651–1657, 1999.

[5] J. H. Hirschenhofer, D. B. Stauffer, R. R. Engleman, and M. G. Klett, *Fuel Cell Handbook*: U. S. Department of Energy, 1998.

[6] J. Ding, P. S. Patel, M. Farooque, and H. C. Maru, "A computer model for direct carbonate fuel cells," in *Proceedings of the Fourth International Symposium on Carbonate Fuel Cell Technology*, Montreal, Quebec, 1997.

[7] C. D. Holland, *Fundamentals of Chemical Reaction Engineering*, New Jersey: Prentice-Hall, 1989.

[8] Fuel Cell Engineering Corporation, Santa Clara, 2MW Fuel Cell Demonstration Power Plant Test Report, prepared for EPRI, TR-108 252, July 1997.

[9] M. D. Lukas, K. Y. Lee, and H. Ghezel-Ayagh, "Operation and control of direct reforming fuel cell power plant," in *Proceedings of the IEEE Power Engineering Society Winter Meeting*, Jan. 2000.

Michael D. Lukas received the B.S. degree in 1987 and the M.S. degree in 1995, both in electrical engineering from the Pennsylvania State University. He is currently pursuing the Ph.D. degree in electrical engineering at the Pennsylvania State University, where he has worked as an instructor in the department. His current research interests include modeling and intelligent control of power plants and carbonate fuel cell systems for stationary and marine power.

Kwang Y. Lee received the B.S. degree in electrical engineering from Seoul National University, Seoul, Korea, in 1964, the M.S. degree in electrical engineering from North Dakota State University, Fargo, in 1968, and the Ph.D. degree in system science from Michigan State University, East Lansing, in 1971. He has been on the faculties of Michigan State, Oregon State, Houston, and the Pennsylvania State University, where he is now Professor of Electrical Engineering. He is currently in charge of the Power Engineering Program and the Power System Control Laboratory at Penn State. His interests are power systems control, operation and planning, and intelligent systems applications. Dr. Lee has been a senior member of IEEE Control System Society, Power Engineering Society, and Systems, Man and Cybernetics Society. He is also a registered Professional Engineer.

Hossein Ghezel-Ayagh received the B.S. degree in chemical engineering from Abadan Institute of Technology, Abadan, Iran, in 1975, the M.S. degree in 1977, and the Ph.D. degree in 1981, both in chemical engineering from Illinois Institute of Technology. He has been involved in research activities related to molten carbonate, phosphoric acid and solid polymer electrolyte fuel cells at FuelCell Energy, Inc., Danbury, CT. He has also been engaged in evaluation and design of power plant systems using various types of fuels such as natural gas, coal gas and heavy hydrocarbons. In addition to process design, his background includes simulation and mathematical modeling of the electrochemical systems. He is a member of the technology team involved in development of 2.85 MW commercial carbonate fuel cell power plant for distributed generation. He has also been involved in the design and successful operation of the world's first MW scale carbonate fuel cell power plant, Santa Clara Demonstration Project (SCDP), in California. He is currently conducting design efforts in the development of direct carbonate fuel cell power plants for marine application.